Response of restrained stainless steel corrugated web beams at elevated temperature

Mustesin Ali Khan[1], Aatif Ali Khan[1], Katherine A. Cashell[2], Asif Usmani[1]

[1]*Department of Building Services Engineering, The Hong Kong Polytechnic University, Kowloon, Hong Kong*

[2]*Department of Civil Engineering, Brunel University London, United Kingdom*

Abstract

This paper is focused on the fire behaviour of axially restrained corrugated web beams made from stainless steel. A finite element (FE) model is developed and validated against available fire test results on restrained flat web carbon steel beams, unrestrained stainless steel cellular beams and numerical studies conducted on carbon steel corrugated web beams in fire. The verified FE model is then employed to conduct an extensive parametric study to assess the relative influence of key properties on the response. The behaviour of stainless steel corrugated web beams (SSCWBs) is compared to that of stainless steel flat web beams (SSFWBs) during exposure to a standard fire under axially restrained support conditions. The axial compression developed in an SSCWB is shown to be significantly lower than that of a comparable SSFWB due to the reduced axial stiffness. A number of parameters are examined including the grade of steel, load ratio, presence of axial restraint as well as thicknesses of the flange and web. It is shown that the overall behaviour of SSCWBs is quite similar compared with equivalent carbon steel corrugated web beams (CSCWBs). However, the stainless steel beams also show much improved performance in terms of survival time due to better retention of mechanical properties at elevated temperature compared with carbon steel. An analytical model for predicting the critical parameters related to the axial force-temperature response of SSCWBs is also presented and verified against the results obtained from the FE models.

Keywords: Stainless steel, corrugated web beams, fire, catenary action, transition temperature

1. Introduction

The construction sector is gradually evolving and improving for a number of reasons including an ever-increasing demand for greater sustainability and resilience, the readier availability of sophisticated technologies and also the relatively less rigid regulatory environments that permit architects and engineers to design with new freedoms. While stainless steel is arguably a sustainable material given its long maintenance-free life cycle, corrosion resistance and resilience, it is yet to be considered a serious alternative to carbon steel in everyday structural applications. It is primarily used as an architectural material in facades or roofing [1] but is not commonly used as a structural material [2] unless corrosion resistance and/or its aesthetic qualities are a requirement. One reason for this is the common perception amongst engineers that stainless steel is prohibitively expensive, but other issues such as a lack of design guidance and standardised sections, confusion over the various grades and their availability as well as a poor understanding of the benefits of stainless steel among structural engineers have traditionally limited its use [3].

Structural members made with stainless steel possess high aesthetic value, good durability, low maintenance costs, excellent sustainability and recycling credentials as well as very good fire resistance, ductility and impact resistance. On the basis of these advantages, it has been shown, that the use of stainless steel can lead to significant savings in terms of the whole-life costs when compared to carbon steel [4]. Test data have consistently shown that stainless steel retains more of its strength and stiffness at higher temperatures compared with carbon steel [5]. Xing et al. [6,7] have conducted experiments and numerical studies to understand the response of stainless steel I-section under fire exposure. In addition to the mechanical characteristics, the thermal properties such as thermal conductivity and heat capacity are also important to determine the temperature history of a structural member subjected to fire. The thermal conductivity of stainless steel is generally lower than that of carbon steel, ranging from 15 W/mK at room temperature to 30 W/mK at 1200°C. In comparison, the thermal conductivity of carbon steel at room temperature is 53 W/mK reduced to 27 W/mk at 800°C based on Eurocode specifications [5].

Corrugated web beams have become increasingly popular for long-spanning structural elements in various applications such as multi-storey buildings, sports arenas, and terminals. Corrugated web beams are typically fabricated using light gauge corrugated web panels which are welded to the flat flange plates. Due to the profiled web, the web's contribution to the longitudinal transfer of bending stresses is negligible and these stresses are carried by the flanges. On the other hand, the transverse forces are resisted by the corrugated web. Corrugated web beams with the same depth and flange area as equivalent flat web beams provide almost identical bending moment resistance and there is no need to provide web stiffeners as the local buckling strength of the web is enhanced by the corrugations [8]; this is the key advantage of these members. In 1906, Elgaali et al. [9,10] performed experimental and numerical studies to estimate the shear and bending strength of beams with a corrugated web. Driver et al. [11] conducted experiments to investigate the shear buckling behaviour of corrugated web bridge girders. The effect of web geometric imperfections was incorporated in the proposed design expression which accounts for both local and global buckling of the corrugated web. Luo and Edlund [12,13] performed a buckling analysis and estimated the shear capacity of girders with the trapezoidal corrugated web.

There are only a handful of studies on the behaviour of CSCWBs exposed to fire, and no information, to date, on the fire response of SSCWBs. Though there are many studies conducted to understand the structural response of carbon steel members under fire exposure [14–17]. Kim et al. [18] performed fire resistance tests on prestressed composite beams with corrugated webs and slim floor beams. They concluded that the fire resistance of more than 3 hours can be achieved by adjusting the size of the section and type of the corrugated web without using any fire protection. Maslak et al. [19] presented a design method to estimate the shear buckling resistance of corrugated web beams under fire exposure. A numerical study was conducted by Wang et al. [20,21] to study the large deflection behaviour of restrained corrugated web steel beams exposed to non-uniform and uniform temperature distribution across the section. Factors such as the load ratio, level of axial restraint, and the span–depth ratio were found to greatly influence the catenary action behaviour of the restrained corrugated web steel beams in a fire.

Most of the structural fire tests conducted to date and discussed in the available literature are on isolated components. These tests fail to capture the effects of the adjoining structure on the

fire exposed element. This is particularly important during fire scenarios because indirect loading may be induced due to the restraint provided to thermal expansion by the surrounding structures. The axial restraint provided by the adjoining structure allows the development of catenary action in the beam at elevated temperature and the load-carrying mechanism gradually changes from bending to behaviour more comparable to a suspended cable. Therefore, the failure temperature of a restrained steel beam in a fire can be significantly higher than that of an equivalent unrestrained beam. However, due to a lack of suitable performance-based design methods, this beneficial catenary effect is generally ignored by structural fire engineers. Recently, there have been a number of studies conducted to understand the development and contribution that is made by catenary action in restrained beams at elevated temperature [22–25]. In addition, virtual hybrid simulations were performed by Khan et al. [26–28] to understand the effect of catenary action on the behaviour of restrained composite beams in fire. Simplified design equations were proposed by Yin and Wang [22] to quantify the catenary effect in steel beams exposed to uniform and non-uniform temperature distribution. Najafi and Wang [24,25] conducted an extensive numerical study, and an analytical model was proposed to investigate the effect of catenary action on the behaviour of restrained cellular beams exposed to fire.

In this paper, the fire response of restrained SSCWBs is studied using the finite element analysis method (FEM). A numerical model is developed in ABAQUS [29] and is described in detail. Following validation of the model, it is employed to study the effects of various parameters on the performance of restrained SSCWBs exposed to elevated temperature. The parameters examined include the type of web (flat and corrugated), steel types (carbon steel and stainless steel), load ratio, axial restraint, and thickness of the flange and web. The results obtained from the parametric study are then compared with an analytical method that was developed and is also described herein to predict the fire behaviour of restrained SSCWBs.

2. Finite element model and verification

A numerical study is performed to understand the thermomechanical response of axially restrained SSCWBs exposed to fire. In this study, the commercially available FE software ABAQUS [29] is employed for modelling the SSCWBs in fire. It has previously been used to model the response of stainless steel structural elements in fire, such as beams and columns [30,31]. Due to a lack of test data on the catenary action behaviour of restrained SSCWBs in a fire, validation of the model is conducted in two stages, to verify the accuracy of the numerical model in capturing all of the key behavioural characteristics. First, the fire tests conducted by Liu et al. [32] on restrained carbon steel beams with flat webs are used to verify different aspects of the modelling approach, such as the element type, mesh size, boundary conditions, and the solution process. Then, the results from the numerical investigation conducted by Wang et al. [20] to study the behaviour of carbon steel corrugated web beams (CSCWBs) is employed to validate the numerical approach for this type of cross-section. Detailed descriptions of both the tests [32] and the FE simulations [20] are presented hereafter.

2.1 Tests and numerical models used for validation of the FE model

2.1.1 Restrained carbon steel beams with flat webs in fire [32]

A total of 15 beams were tested by Liu et al. [32] at the Fire Research Laboratory at the University of Manchester. The beams examined had varying load ratios and also levels of axial

and rotational restraint. The tested beams were all 178×102×19 UB (universal beam) sections with a nominal yield strength of 275 N/mm^2. The axial restraint at both ends of the beams was provided using columns made from 152×152×30 (universal column) UC sections also with a nominal yield strength of 275 N/mm^2, forming a structure similar to a 'rugby goalpost' frame, as shown in Fig.1. The axial restraint stiffness developed due to the columns at the beam ends was determined as 8 kN/mm. The axial restraint was increased to 62 kN/m by using struts for external axial restraint, as shown in Fig.1. A rotational stiffness of 14000 kNm/rad was developed at the beam ends using extended end plate connections.

The experiments were conducted under four-point loading conditions with load ratios (LR) of either 0.5 or 0.7. The load ratios were calculated as the ratio of applied bending moment to the plastic moment capacity of the beams at room temperature, assuming simply supported boundary conditions. The span of the tested beam was 2 m, and the point loads were applied at a distance of 0.6 m from each end. For brevity, only the results for the beam with a LR of 0.5 and total axial restraint of 62 kN/m are presented herein to illustrate the accuracy of the modelling approach as similar results were shown for all the other scenarios also.

The tests were performed in two steps. In the first step, the mechanical load was applied at room temperature, and in the second step, the furnace temperature was increased as per the standard fire curve while maintaining the same static load. The temperatures were recorded at the web, bottom flange, and top flange of the beams, as shown in Fig. 2. No fire protection was applied to the web and bottom flange, whereas the top flange was protected by a 15 mm thick ceramic fibre blanket. Other members of the frame, such as the struts providing the axial restraint were also provided with fire protection.

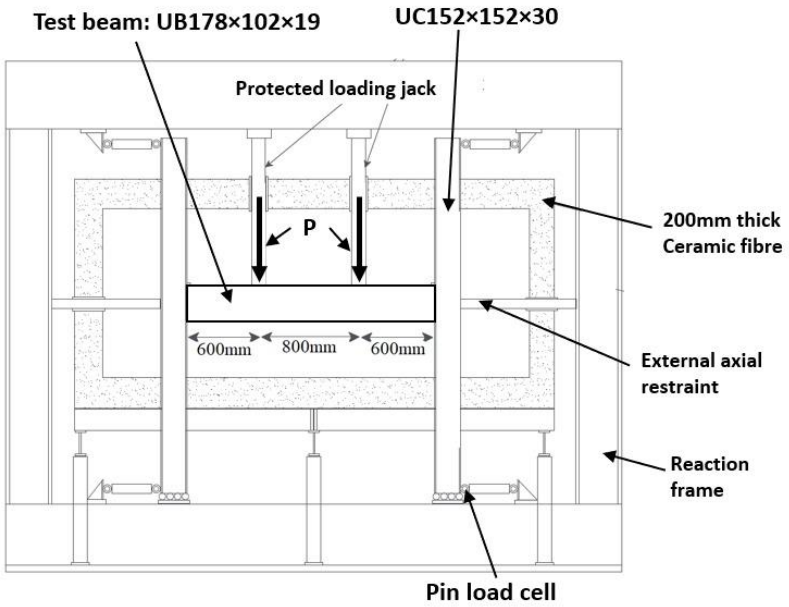

Figure 1 Schematic elevation view of the test assembly used by Liu et al. [32] and Pournaghshband et al. [33]

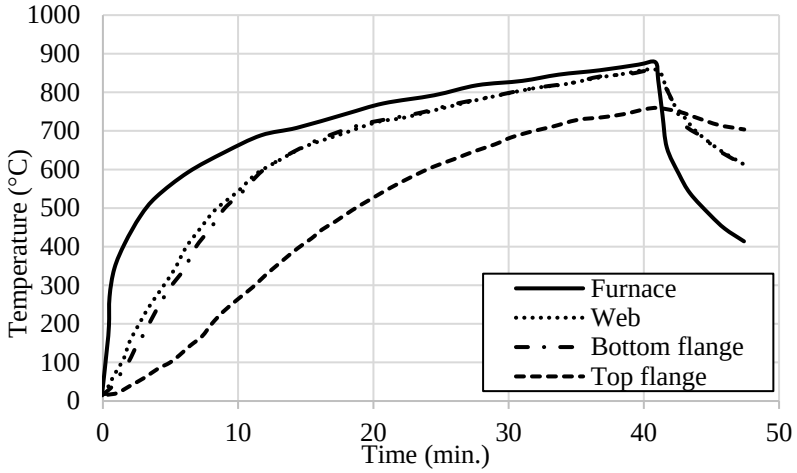

Figure 2 Test temperatures recorded by Liu et al. [32]

2.1.2 Restrained carbon steel corrugated web beams in fire

A numerical study to understand the fire response of carbon steel corrugated web beams (CSCWBs) was performed by Wang et al. [20]. The geometry of the trapezoidal-shaped corrugated web as recommended in CECS 291-2011 [34] is shown in Fig. 3(a). The span of the beam was 9.6 m and there were 80 half waveforms along the length. The level of axial restraint provided at the beam end was assumed to be 10% of the axial stiffness of the beam cross-section. The beam was allowed to rotate about the cross-section major axis while all other degrees of freedom were restrained. The top flange of the beam was restrained laterally to prevent lateral-torsional buckling. In this analysis, the beam had a load ratio of 0.5 and then a uniform temperature distribution was applied to the section.

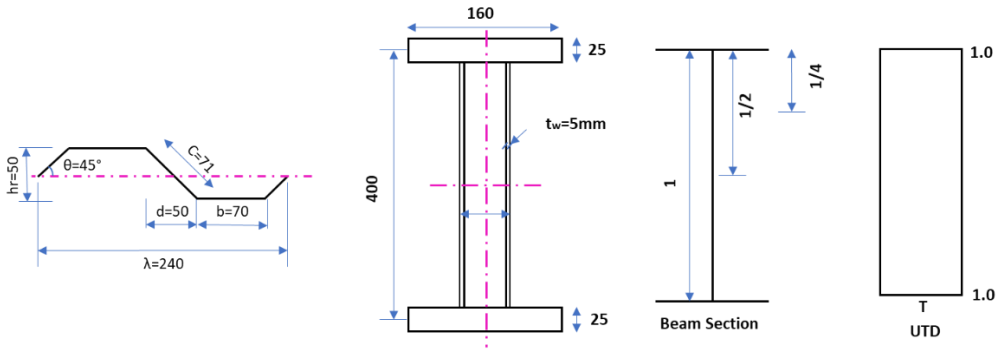

Figure 3 Details of the trapezoidal-shaped corrugated web beam modelled by Wang et al. [20] including (a) the web dimensions (in mm) and (b) the uniform temperature distribution across the section

2.1.3 Stainless cellular beam in fire

A fire test on stainless steel cellular beam was conducted by Cashell et al. [35,36] at Tampere University, Finland. The stainless steel cellular beam was fabricated using stainless steel plates of grade 1.4301. The schematic view of the beam is presented in Fig. 4, showing the opening layout. The beam was tested under simply supported boundary conditions with a span of 4.3 m

and 12 circular openings of 200 mm diameter at 300 mm centre to centre spacings. The test was conducted in two stages. In the first stage, the beam was loaded under a four-point loading arrangement with two point loads of 58 kN each as shown in Fig. 4 (b). Once the static load was applied, the fire load was applied on the beam using a furnace that was programmed to apply temperatures as per the ISO 834 standard fire curve [37]. The midspan vertical deflections and horizontal displacements at the supports were recorded in the test.

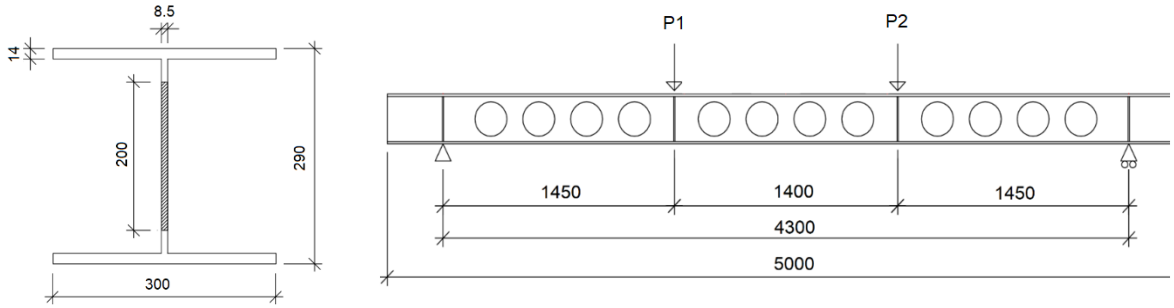

(a) (b)

Figure 4 Schematic of the stainless steel cellular beam [36] (all dimensions are in mm) including (a) the cross-section and (b) an elevation view

2.2 Finite element modelling

The finite element model was developed in ABAQUS and performs a sequential heat transfer and thermomechanical analysis to simulate the tests previously described. The static load is applied to the beams followed by the application of fire. The steel beam is modelled using S4R shell elements (four nodes reduced integration) available in the ABAQUS material library [29]. The thermal properties of the steel such as the thermal conductivity and specific heat are assigned the values recommended in the Eurocodes [5]. As in the physical tests [32], the standard fire time-temperature history [37] is applied at different locations on the steel beam as the thermal boundary conditions. The heat transfer from the gas phase to the structural elements is modelled by applying appropriate convection and radiation boundary conditions. A convection coefficient of 25 W/m^2K is employed for temperature-exposed surfaces and 9 W/m^2K for the other surfaces which are at ambient temperature. An emissivity value of 0.7 is used for carbon steel. The thermal properties of the ceramic fibre blanket used for insulating the top flange are assumed to be the same as those defined by Hua Wang et al. [38]. The temperature-time history obtained from the heat transfer analysis of the beam following exposure to a standard fire is subsequently input into the thermomechanical model as the thermal load to simulate the structural response of the restrained steel beam under fire conditions. An excellent agreement has been obtained between the temperature profiles obtained after conducting heat transfer analysis and the test results as shown in Fig. 5.

The elevated temperature mechanical properties for carbon steel as given in EN 1993-1-2 [5] are employed in the model. To apply the required axial and rotational restraint, a reference point is defined on the centroidal axis of the section. All of the nodes at the beam-end cross-section are connected to the reference point using a coupling constraint, as shown in Fig. 6. Then, this reference point is assigned with the appropriate boundary conditions. For a restrained beam, all of the degrees of freedom are restrained except for the longitudinal translation and rotation about the cross-sectional major axis. In the tests, the end connections were estimated to provide

a rotational restraint of 14,000 kNm/rad, which is simulated using a rotational spring with an identical stiffness in the model. The total axial restraint of 62 kN/m is also applied using a translational spring.

The thermomechanical analysis is performed in two steps. In the first step, the static load corresponding to a load ratio of 0.5 is applied at ambient temperature. Then, in the second step, the temperatures recorded during the heat transfer analysis are applied and the static load is maintained on the beam. The axial force *versus* temperature and deflection *versus* temperature behaviours obtained from the FE simulations are compared with the test results in Fig. 7. It is shown that the model is able to provide a realistic and accurate depiction of the real behaviour. Fig. 8 presents the deformed shapes of the restrained beam obtained from both the test and the FE model. The bottom flange buckling occurred mainly due to the high level of compressive axial reaction developed at the support due to restrained thermal expansion. Thermal bowing is also responsible for the bottom flange buckling as the bottom flange was not provided with any fire protection and expanded more compared to the top flange. Again, it is shown that a reasonably good agreement is obtained between the test results and FE simulations.

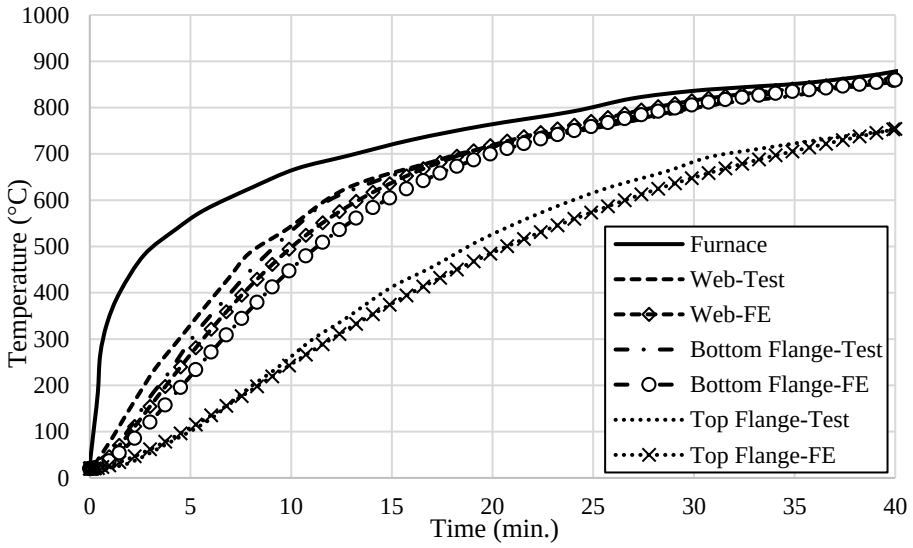

Figure 5 Comparison of FE temperature with test temperatures recorded by Liu et al. [32]

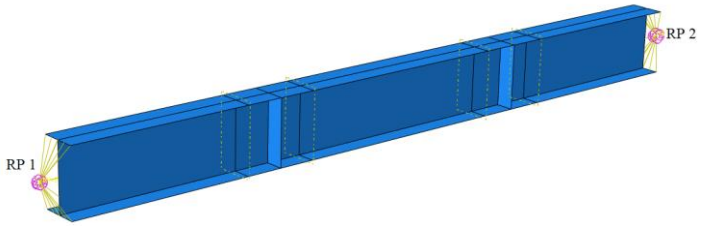

Figure 6 Boundary conditions in the thermomechanical model

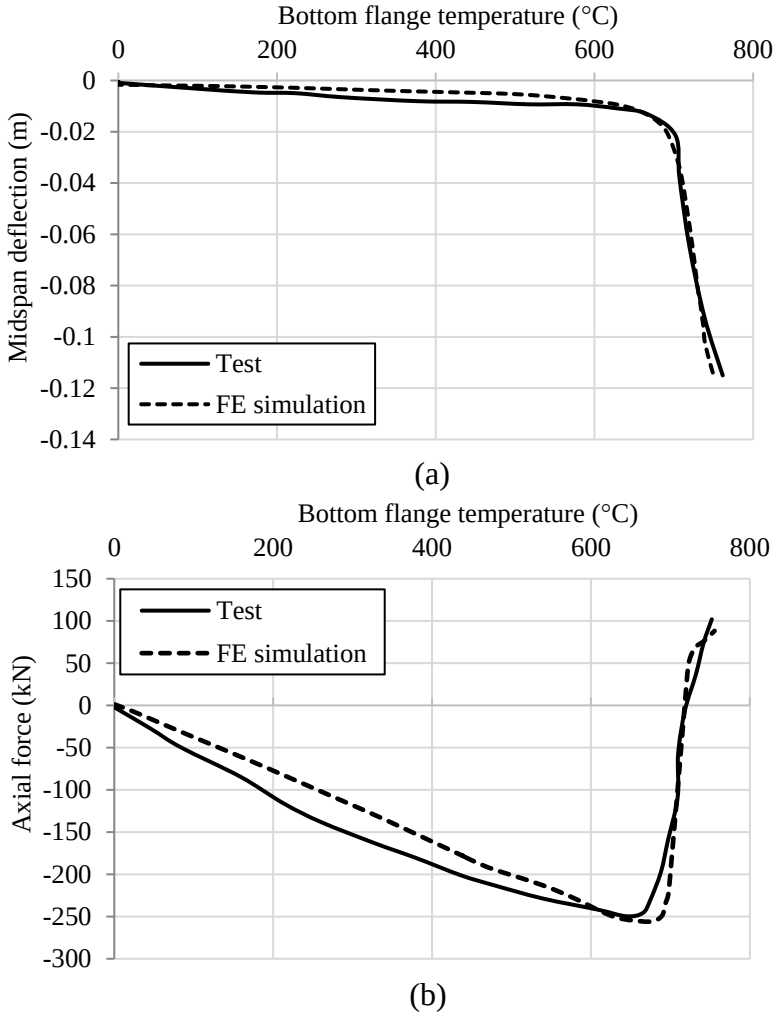

Figure 7 Comparison of the test and FE data including (a) vertical deflection *versus* temperature and (b) axial force *versus* temperature responses from test [32] and FE simulation

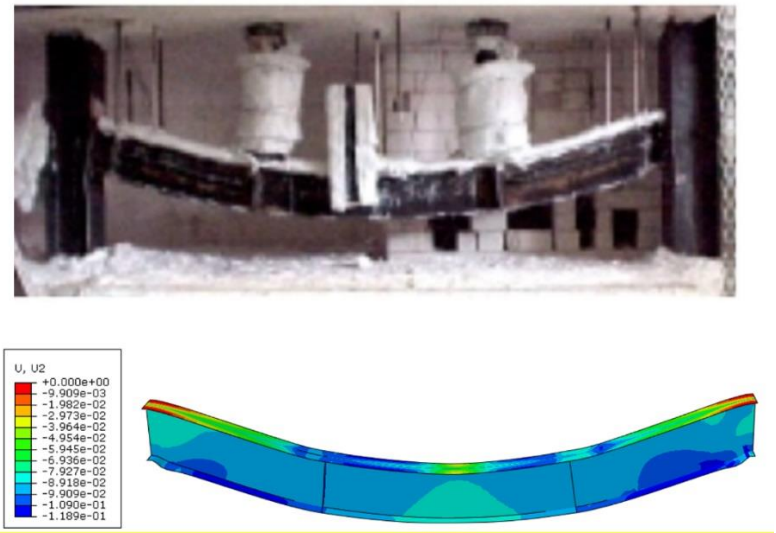

Figure 8 Comparison of the deformed shape obtained from the test and from [32] the FE simulation

The numerical analysis performed by Wang et al. [20] to understand the fire response of carbon steel corrugated web beams (CSCWBs) is also simulated using ABAQUS herein, to validate the numerical approach for this type of cross-section. As stated before, the geometry of the trapezoidal-shaped corrugated web cross-section is as shown in Fig. 3(a) and the beam has a span of 9.6 m with 80 half waveforms along the length. The level of axial restraint provided at the beam end is assumed to be 10% of the axial stiffness of the beam cross-section. The beam is allowed to rotate about the cross-section major axis while all other degrees of freedom are restrained. The top flange of the beam is restrained laterally to prevent lateral-torsional buckling. The support boundary conditions are applied at the reference point, as shown in Fig. 9.

In the first step, a uniformly distributed load of 143.6 kN/m^2 corresponding to a LR of 0.5 is applied. In the second step, a uniform temperature distribution (UTD) across the section is implemented, as shown in Fig. 3(b). The vertical deflection and axial force behaviour of the CSCWB obtained from the simulation is compared with the results presented by Wang et al. [20] in Fig. 10, and it is shown that a good agreement is obtained. It is shown that the load-carrying mechanism of CSCWBs is similar to that of flat web restrained steel beams. Therefore, in the initial stages of the fire, the load-carrying mechanism changes from beam bending to behaviour more similar to a beam-column as the compressive force develop in the section due to the restrained axial expansion. With further temperature increases, the beam eventually behaves in a catenary, similar to a suspended cable. Following successful validation of the numerical approach against two independent sets of data, in the following sections, the finite element model is employed to perform parametric studies on axially restrained SSCWBs in fire.

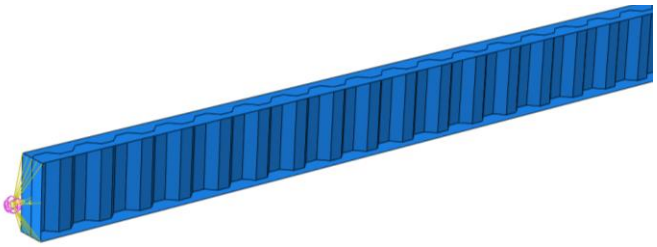

Figure 9 Boundary conditions for the corrugated web beam model

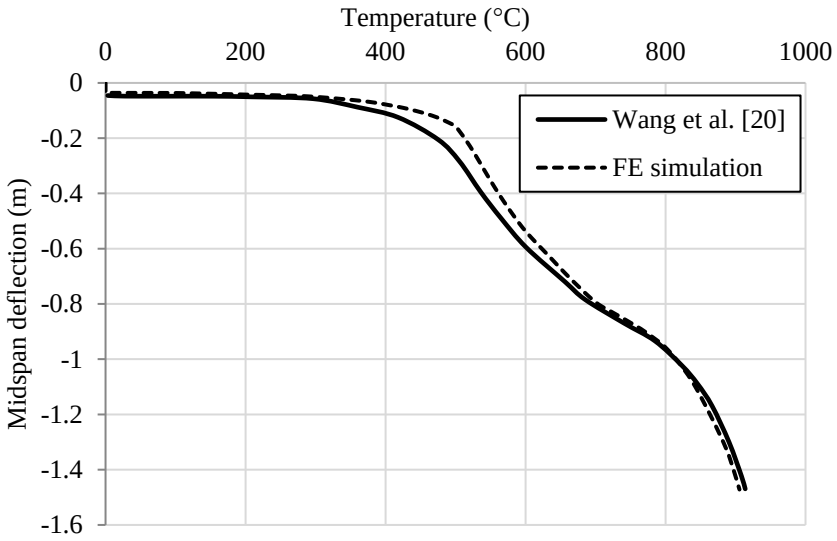

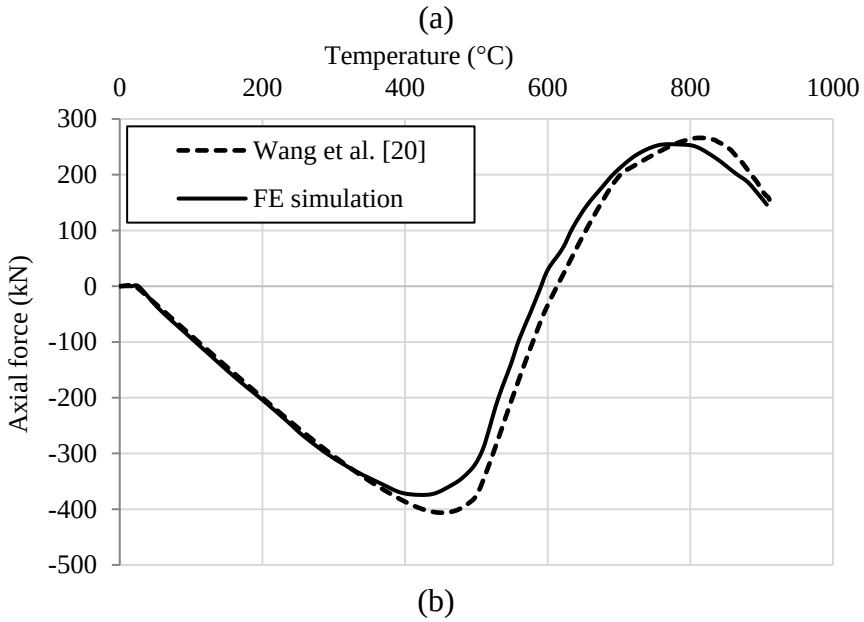

Figure 10 Comparison of the FE model predictions with those shown by Wang et al. [20] for the fire response of carbon steel corrugated web beams including (a) vertical deflection *versus* temperature and (b) axial force *versus* temperature

A numerical model using FE software ABAQUS is developed to validate the behaviour of stainless steel cellular beams in fire that was tested by Cashell et al. [36]. Shell elements (S4R) available in ABAQUS library are employed to model the cellular beam. Simply supported end conditions are adopted in the model to replicate those in the test, by restraining the appropriate displacement and rotation degrees of freedoms. The stainless steel mechanical properties for austenitic grade 1.4301 at room temperature and elevated temperature are employed as per the modified Ramberg-Osgood model as presented by Eqs. 1 and 2 and also recommended in the SCI design manual for structural stainless steel [39]. Details of the stainless steel material properties at elevated temperature used in numerical modelling are provided in section 3. Similar to the test, the FE analysis is performed in two stages. In the first stage, two point loads of 58 kN each are applied. Then, the average temperatures extracted from the test are applied at various locations such as the top flange, bottom flange and web as shown in Fig 11. The temperature gradient across the section as presented in Fig 11 is applied uniformly along the entire length of the beam. Clearly, an excellent agreement has been obtained between the numerical model and the test results as shown in Fig. 12. The FE model can accurately predict critical phenomena such as large deflections due to significant degradation in material properties at the later stages of the analysis. The minor discrepancies in the early stages are attributed to some initial movement in the test specimen upon the application of mechanical loads.

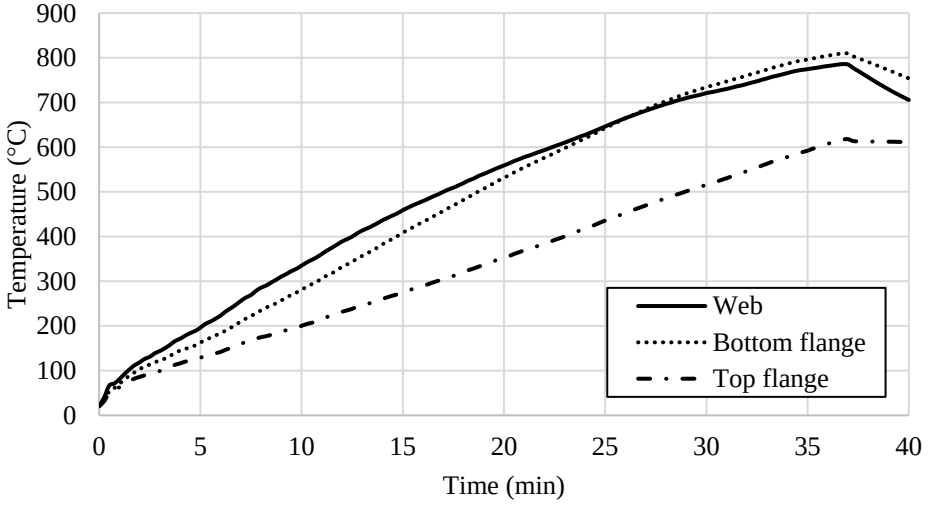

Figure 11 Average test temperatures recorded by Cashell et al. [36]

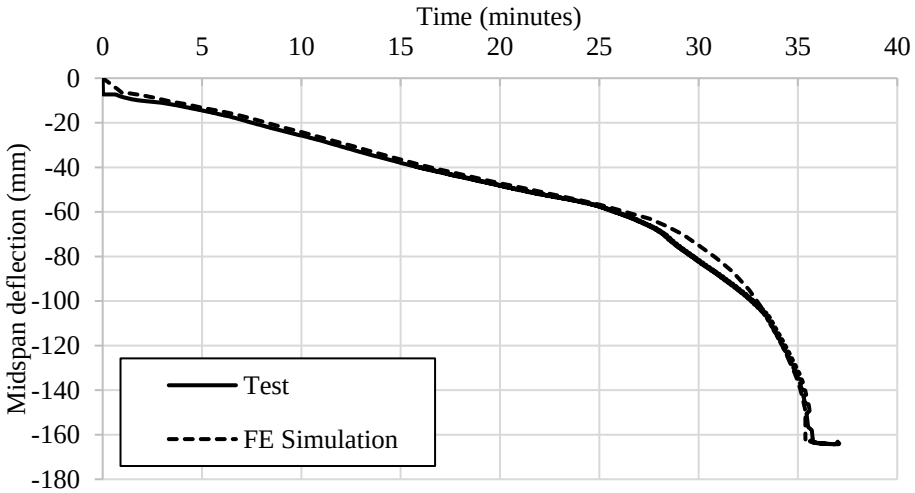

(a)

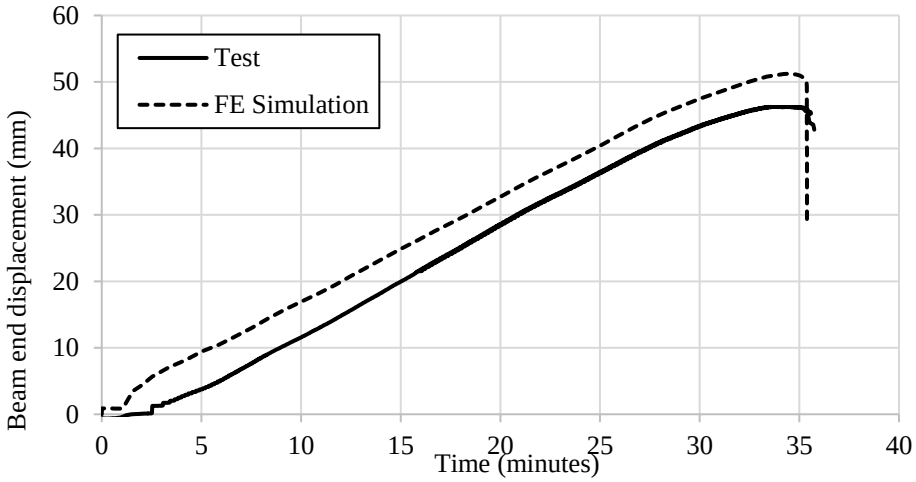

(b)

Figure 12 Comparison between the experimental results [36] and FE simulations for (a) mid-span deflection versus time and (b) end displacements versus time

3. Behaviour of stainless steel *versus* carbon steel corrugated web beams

In the previous section, the FE model was verified and shown to reliably simulate the behaviour of restrained flat web and corrugated web steel beams. In this section, the overall response including the axial force and midspan deflection behaviour is studied and compared for SSCWBs and CSCWBs exposed to fire. The same model developed for CSCWBs in the previous section is employed here to model the SSCWBs, with an appropriate material model. It is assumed that the SSCWBs are made using grade 1.4401 austenitic stainless steel and the corresponding strength and stiffness reduction factors are taken from the SCI design manual for structural stainless steel [39]. The stress-strain response of stainless steel at room and elevated temperatures is modelled using the two-stage Ramberg-Osgood model which is also recommended in the SCI design manual for structural stainless steel [39], and is given in Eqs.1 and 2:

$$\varepsilon_\theta = \frac{\sigma_\theta}{E_\theta} + 0.002\left(\frac{\sigma_\theta}{\sigma_{0.2,\theta}}\right)^{n_\theta} \quad for\ \sigma_\theta \le \sigma_{0.2,\theta} \qquad (1)$$

$$\varepsilon_\theta = \frac{\sigma_\theta - \sigma_{0.2,\theta}}{E_{0.2,\theta}} + \varepsilon_{u,\theta}\left(\frac{\sigma_\theta - \sigma_{0.2,\theta}}{\sigma_{u,\theta} - \sigma_{0.2,\theta}}\right)^{m_\theta} + \varepsilon_{0.2,\theta}\ for\ \sigma_{0.2,\theta} < \sigma \le \sigma_{u,\theta} \qquad (2)$$

where θ is the temperature, σ_θ and ε_θ are the engineering stress and strain at θ, respectively, E_θ is the modulus of elasticity at θ, $f_{y,\theta}$ and $\varepsilon_{y,\theta}$ are the yield stress and strain at θ, respectively, $E_{0.2,\theta}$ is the tangent modulus at θ, $f_{u,\theta}$ and $\varepsilon_{u,\theta}$ are the ultimate stress and strain at θ, respectively, and n_θ and m_θ are strain hardening constants. It is assumed that the beam is exposed to a standard fire in terms of the fire load, in accordance with the values given in Eurocode 1 Part 1-2 [37]. The convective heat transfer coefficient and the emissivity for stainless steel are taken as 25 W/m^{2}K and 0.4, respectively. The thermal properties such as specific heat, thermal expansion and thermal conductivity are taken from the guidance given in the SCI design manual [39] for grade 1.4401 stainless steel.

As before, the simulation is run in two steps. Firstly, the member (either a SSCWB or CSCWB) is loaded with a uniformly distributed load (UDL) corresponding to a LR of 0.3. In the second step, the temperature history is applied at all locations along the length of the beam. It its noteworthy that the top flange of the beam is restrained laterally in order to prevent lateral-torsional buckling failure. Fig. 13 presents (a) the vertical deflection *versus* temperature behaviour and (b) the axial force *versus* temperature, for SSCWBs and CSCWBs with varying levels of axial restraint between 5% and 100% of the axial stiffness of the beam. The graphs also include the results for fully fixed beams. There are a number of interesting observations from these graphs. Firstly, it is clear that during the initial stages of the fire, the vertical deflections in the SSCWBs as shown in Fig. 13(a) are higher compared to CSCWBs. This is attributed to the higher coefficient of thermal expansion of stainless steel compared with carbon steel. For all beams, local buckling or yielding occurs in the most highly stressed locations of the beam under the compressive forces which develop due to restrained thermal expansion. This causes an unloading of the compression force as the temperature increases further, resulting in

greater deflections and ultimately runaway behaviour. The stage at which local buckling or yield occurs is dependent on both the level of axial restraint that is provided and also the material that the beam is made from, as stainless steel and carbon steel have different elevated temperature mechanical properties. When both types of beam have relatively low degrees of axial restraint provided (i.e. up to 10%), the level of axial compressive force required to cause local buckling or yielding and then runaway behaviour does not occur until the temperature in the beam is around 400°C. At this temperature and above, the mechanical properties of stainless steel are better than those of carbon steel, in that they maintain more of their original strength and stiffness. Therefore, failure of the stainless steel corrugated web beams occurs later, at higher temperatures, compared with their carbon steel equivalents. On the other hand, when the corrugated web beams are subjected to axial restraint which is 30% of the axial stiffness of the beam or above, the level of compressive force required to cause local buckling or yielding in the section leading to runaway failure occurs at temperatures which are less than 400°C as shown in Fig. 13(a). In this temperature range, the mechanical properties of carbon steel are better than those of stainless steel and therefore runaway failure occurs at a relatively lower temperature for the SSCWBs compared with CSCWBs.

With reference to Fig. 13(b), it is shown that during the early stages of the fire, the axial compressive force increases at a higher rate in the SSCWBs compared to CSCWBs for all levels of axial restraint provided, which is also attributed to the higher thermal expansion of stainless steel. The load-carrying mechanism changes from flexure to tensile catenary action at a temperature of around 850°C for the SSCWBs and 630°C for the corresponding CSCWBs. The relative delay in reaching catenary action for the SSCWBs relative to the CSCWBs is due to the fact that stainless steel retains more of its strength and stiffness compared with carbon steel at higher temperatures. This is also the reason that ultimate failure occurs later for SSCWBs compared to CSCWBs. It is noteworthy that the maximum tensile force in the section which occurs at failure is similar for both types of beam due to the comparable residual ultimate tensile strength of these beams.

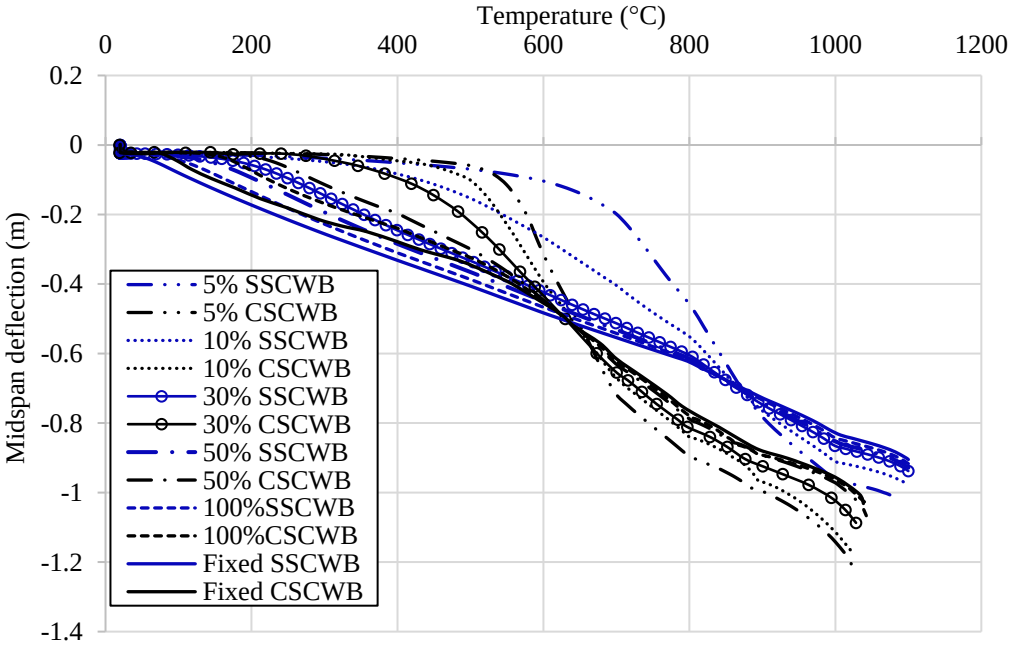

(a)

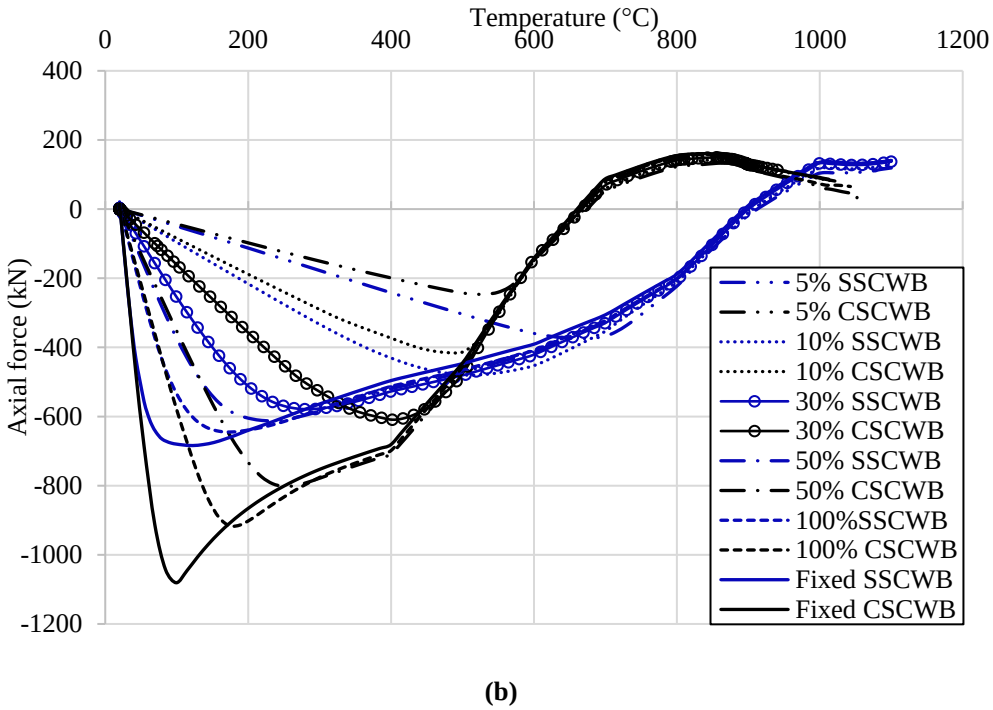

(b)

Figure 13 Comparison of the behaviour of SSCWBs and CSCWBs with various levels of axial restraint at elevated temperature including (a) the vertical deflection *versus* temperature and (b) the axial force *versus* temperature.

4. Behaviour of flat web *versus* corrugated web stainless steel beams

In this section, the elevated temperature behaviour of SSCWBs is compared to that of regular stainless steel beams with a flat web. The axial stiffness of SSCWBs is significantly lower than that of SSFWBs as the corrugated web makes almost no contribution towards the axial stiffness of the section. The FE model developed earlier is employed for this analysis and therefore the same beam dimensions are utilised, as shown in Fig. 3(a). In the first step, both beams are loaded under a UDL corresponding to a LR of 0.3. In the second step, the thermal load is applied in accordance to the standard fire exposure. An axial restraint corresponding to 50% of the axial stiffness of the beam (i.e. AE/L, where A is the cross-sectional area, E is the elastic modulus and L is the beam length) is applied for both the standard beam and the corrugated web beam. The temperature *versus* midspan deflection responses are shown in Fig. 14(a), where a very similar response is observed for both beams. In this figure, CW indicates the beam with a corrugated web whilst FW represents the beam with a flat web. This is because the main contributors to the flexural stiffness of the section are the flanges, which are identical, and the contribution from the web is negligible. In both cases, typical restrained beam behaviour with the development of catenary action is observed as the temperature increases.

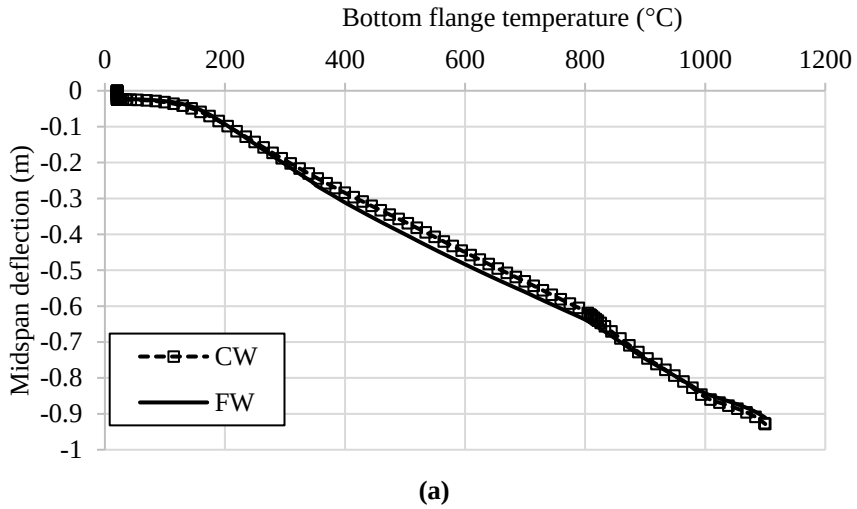

(a)

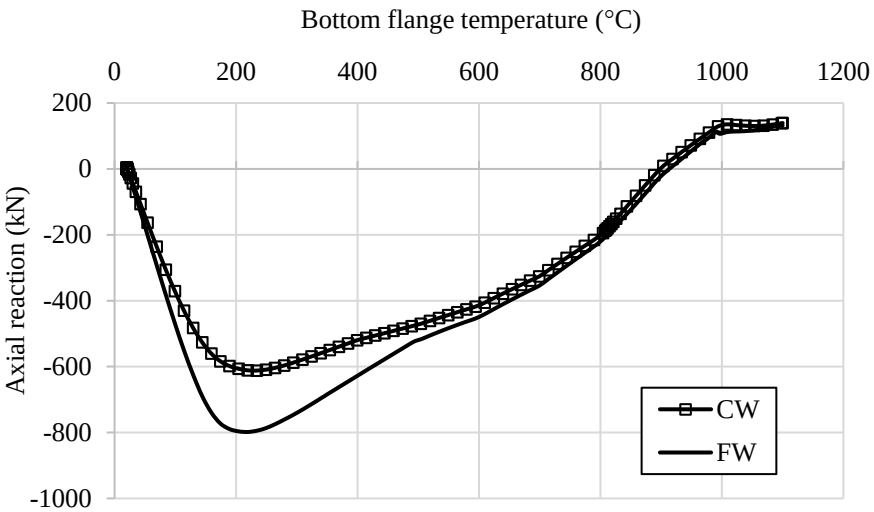

(b)

Figure 14 Comparison of the behaviour of stainless steel beams with either a corrugated web (CW) or a flat web (FW) including (a) the vertical deflection *versus* temperature and (b) the axial force *versus* temperature.

Fig. 14(b) presents the variation in axial force that develops in both beams as the temperature increases. It is shown that initially, the compressive force increases with the rise in temperature due to restrained thermal expansion in the cross-section but the magnitude of the maximum compressive force is greater for the stainless steel beam with a flat web (FW) compared to that with a corrugated web (CW). This is mainly owing to the greater axial stiffness of the beam with a flat web compared with the corrugated web beam. As soon as local buckling or yielding occurs in both types of beam, unloading of the compression force in the section begins and the axial force changes from compression to tension as catenary action dominates the behaviour. The transition temperature at which the load-carrying mechanism changes from flexure to tension is also similar for both types of beam as the flexural resistance is mainly determined by the properties of the flanges.

5. Parametric study

Following on from the earlier analysis in which the influence of the material type and web shape have been examined, in the current section, the FE model is employed to conduct a detailed parametric study to assess the relative influence of a range of key parameters on the fire performance of restrained SSCWBs. The effect of axial restraint, load ratio, flange thickness and web thickness on the axial and flexural behaviour of SSCWBs is studied. In total, seven different levels of axial restraint are considered (i.e. corresponding to 0%, 5%, 10%, 30%, 50% and 70% of the axial stiffness of the beam, as well as beams with full axial restraint), three different load ratios (equal to 0.3, 0.5 and 0.7), three flange thicknesses (equal to 20, 25 and 30 mm), as well as beams with three different web thicknesses (i.e. 3, 5, and 7 mm). For all of the analyses in this section, it is assumed that the beam has a cross-section as shown in Fig. 3, has a benchmark level of axial restraint corresponding to 50% of the axial stiffness of the section and is subjected to vertical loading corresponding to a load ratio of 0.3 unless otherwise indicated.

5.1 Effect of axial restraint

In this section, seven different levels of axial restraint are applied to the SSCWB, corresponding to 0%, 5%, 10%, 30%, 50% and 70% of the axial stiffness of the beam, as well as members with full axial restraint. Fig. 15 presents (a) the midspan deflection *versus* temperature behaviour and (b) the axial force *versus* temperature response, for all cases. With reference to Fig. 15(a), it is observed that the level of axial restraint provided to the beam is very influential to the overall behaviour in terms of the onset of local buckling or yielding and resulting runaway failure. The runaway behaviour occurs following the onset of local buckling or yielding of the most stressed cross-section due to the compressive force induced in the section as a result of restrained thermal expansion. When the SSCWB is simulated without any axial restraint, axial compression is not induced in the cross-section and therefore local buckling does not occur and runaway is delayed compared with the other scenarios examined. When the beam does experience the large levels of vertical deflection associated with runaway, it is because yielding occurs owing to the reduced strength and stiffness of the stainless steel material at high temperatures.

Generally, the magnitude of the maximum compressive axial force increases for beams with greater levels of axial restraint as this results in local buckling or yielding occurring relatively earlier in the response. The runaway in beams with high levels of axial restraint occurs at lower temperatures compared to those with a lower level of axial restraint, as shown in Fig. 15(a). In the early stages of the response, before the onset of local buckling or yielding, the midspan deflection behaviour is dominated by the magnitude of the compressive force induced in the section, which is dependent on the level of axial restraint provided. On the other hand, in the later stages, when the load-carrying mechanism of the SSCWB changes from flexure to tensile catenary action (which is generally observed to occur at higher temperature range between 700 and 900°C), the behaviour is mainly dominated by the strength and stiffness of the stainless steel.

From Fig. 15(b), it is observed that the transition temperature (i.e. where the beam changes from carrying load through flexural action to tensile catenary action) is very similar for all levels

of restraint examined. In addition, as stated before, the magnitude of the maximum compressive axial force which develops due to the restrained thermal expansion increases when greater levels of axial restraint are provided. It is shown herein that SSCWBs with lower levels of axial restraint develop their maximum compressive force at relatively greater temperatures compared to those with higher levels of axial restraint and hence runaway behaviour is delayed. For example, for the SSCWB with 5% axial restraint, the maximum compressive force (370 kN) develops at 654°C, while the corresponding value for the beam with 70% axial restraint is 631 kN and this occurs at just 198°C. It is relevant to note that very high axial forces can be detrimental to the response of connections under fire exposure and it is clear that both the magnitude of the compressive force as well as the level of elevated temperature are important factors for the design of connections.

Overall, it is concluded that in the early stages of the response, the level of axial restraint greatly influences the midspan deflection behaviour of SSCWBs whilst as the temperature increases and approaches the transition temperature, the effect of axial restraint on the vertical deflection behaviour reduces and the behaviour is governed by the strength and stiffness retained by the stainless steel in the beam.

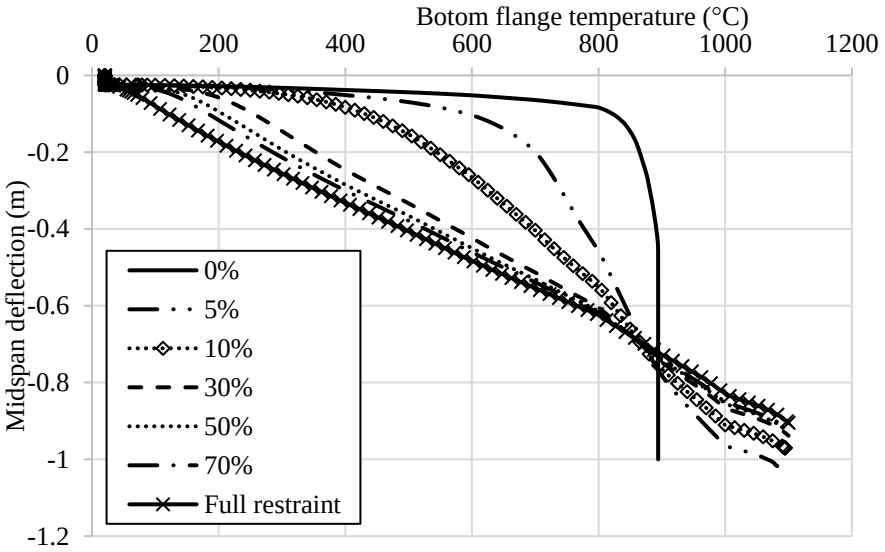

(a)

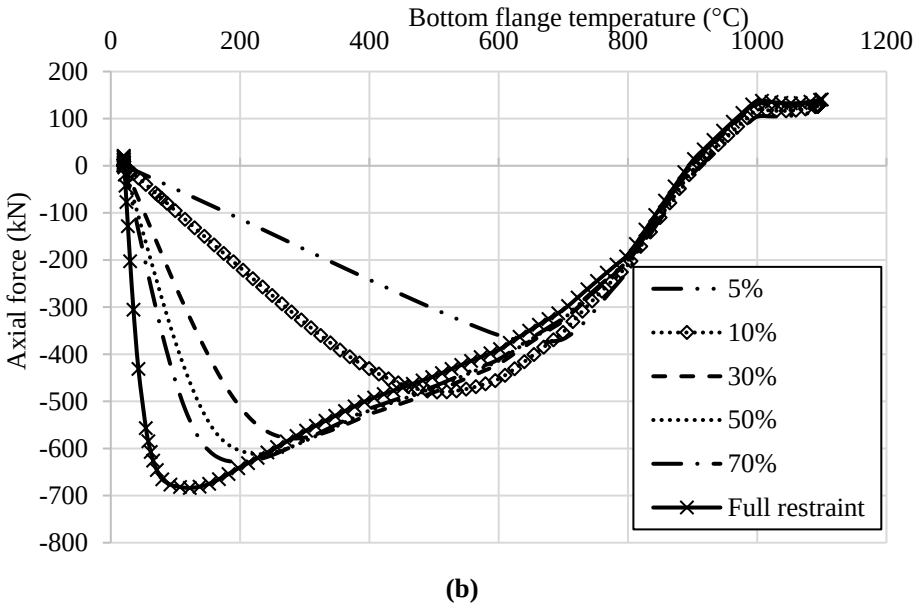

(b)

Figure 15 Influence of the level of axial restraint provided to SSCWBs under fire conditions in terms of (a) the vertical deflection *versus* temperature and (b) the axial force *versus* temperature

5.2 Effect of the load ratio

Three different load ratios LR equal to 0.2, 0.5 and 0.7 are applied to the SSCWB to examine the influence that this parameter has on the elevated temperature response. As stated before, it is assumed that the axial restraint provided to the beam is equal to 50% of the axial stiffness of the section. The results are presented in Fig. 16 and it is observed that, as expected, SSCWBs with higher load ratios experience greater deflections during the first step, before the fire begins. As the temperature increases, the overall midspan deflection behaviour is similar to that observed in earlier sections of this paper. Overall, at elevated temperature, the level of vertical deflection is greater for beams with a higher LR. It is observed that at ambient temperature, the axial force induced in the section is tensile when the beam is subjected to a relatively high LR (i.e. LR of 0.7), while at lower load ratios (i.e. LR equal to 0.3 or 0.5), the axial force developed at room temperature is almost zero. Then, as the temperature in the section rises, the axial force changes to compression owing to the restraint provided when the beam experiences thermal expansion. The maximum compressive force induced in the section is greater for SSCWBs with a relatively lower LR, as shown in Fig. 16(b). When the temperature of the beam increases, it tends to push the support outwards, but due to the restraint provided, a compressive force is induced in the section. On the other hand, when the beam has a relatively high LR of 0.7, there are greater vertical deflections that tend to pull the support inwards. Therefore, for beams with a higher LR, there is a lower overall level of axial compressive force in the beam, as shown in Fig. 16(b). Due to this effect, SSCWBs with higher LRs reach the tensile catenary action phase of the response earlier compared with identical beams with a lower LR. The magnitude of the ultimate tensile force is also affected by the load ratio, and it is greater for SSCWBs with higher load ratios due to the pull-in effect under vertical loading.

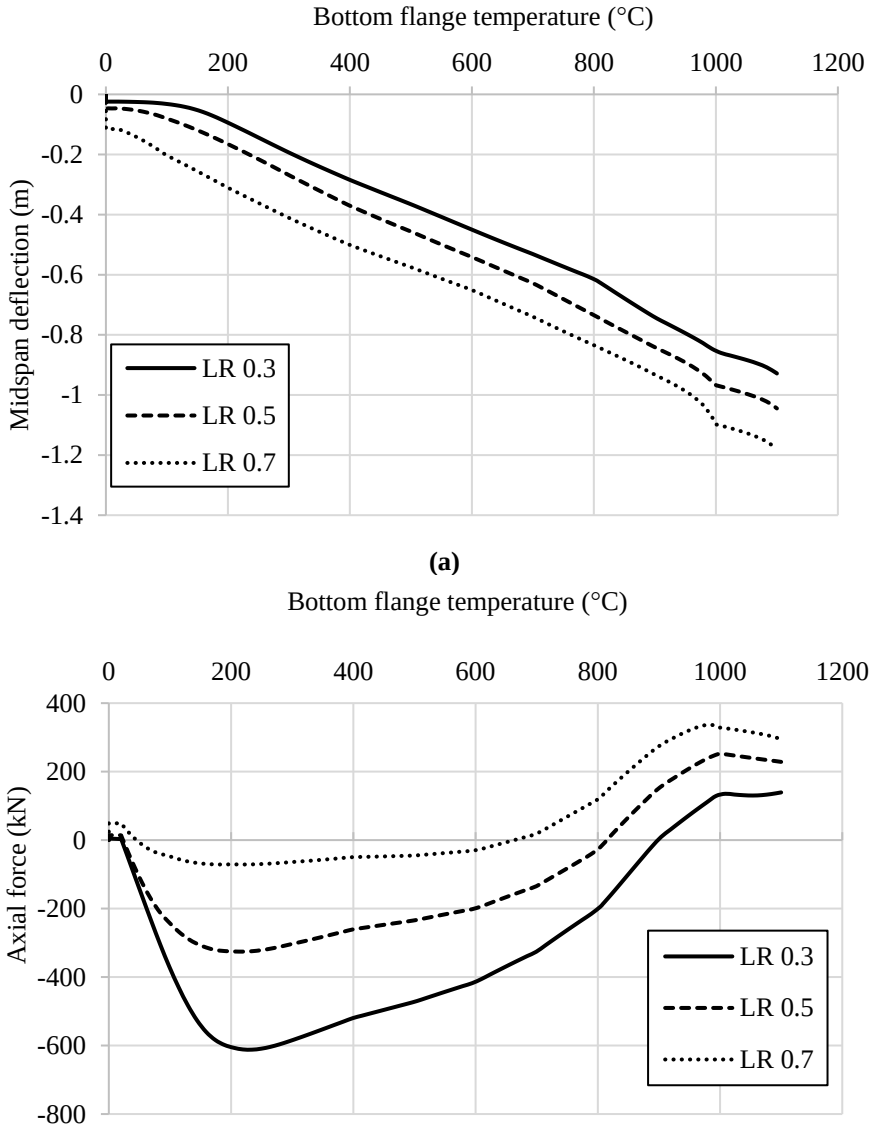

Figure 16 Influence of the load ratio on the elevated temperature behaviour of SSCWBs in terms of (a) the vertical deflection *versus* temperature and (b) the axial force *versus* temperature

5.3 Influence of flange thickness

The properties of the beam flanges are highly influential to both the flexural and axial stiffness of the SSCWB section, as the corrugated web makes only a negligible contribution. Accordingly, in this section, the effect that the flange thickness has on the elevated temperature response of axially restrained SSCWBs is examined. Three different flange thicknesses (both top and bottom flanges) are examined, equal to 15, 20, 25, 30 and 35mm, respectively, and the results are presented in Fig. 17. It is observed that the onset of runaway deflection occurs at a relatively lower temperature when the flange is comparatively thin, as local buckling or yield occurs sooner. For SSCWBs with a thicker flange, the magnitude of the compressive axial force developed is also higher due to the higher axial stiffness of this section. For example, the maximum compressive forces are 1015 kN and 200 kN for the SSCWBs with flanges that are

35 and 15 mm in thickness, respectively. The critical temperature at which the load-carrying mechanism changes from flexure to tension is relatively higher for members with thicker flanges, as shown in Fig. 17(b), due to the greater axial capacity of these sections. It is noteworthy that for the range of beam geometries examined herein, the maximum axial tensile force in the section for members with a relatively low LR of 0.3 is not greatly affected by the flange thickness as all of the members are capable of resisting the maximum tensile forces that develop under this loading condition. On the other hand, for the beams with a LR of 0.5 or above, the maximum tensile force that develops in the section is dependent on the flange thickness and the sections with greater cross-sectional areas can resist greater tensile loads, as expected.

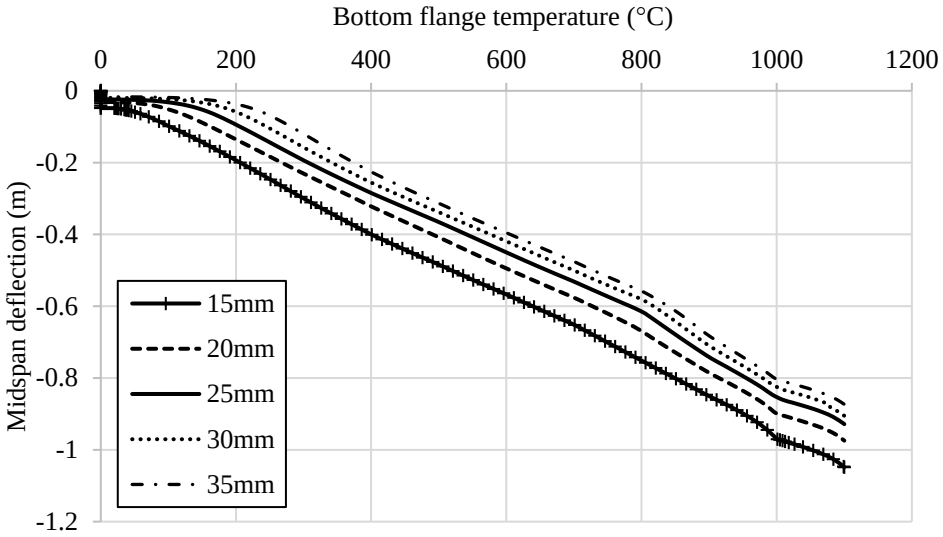

(a)

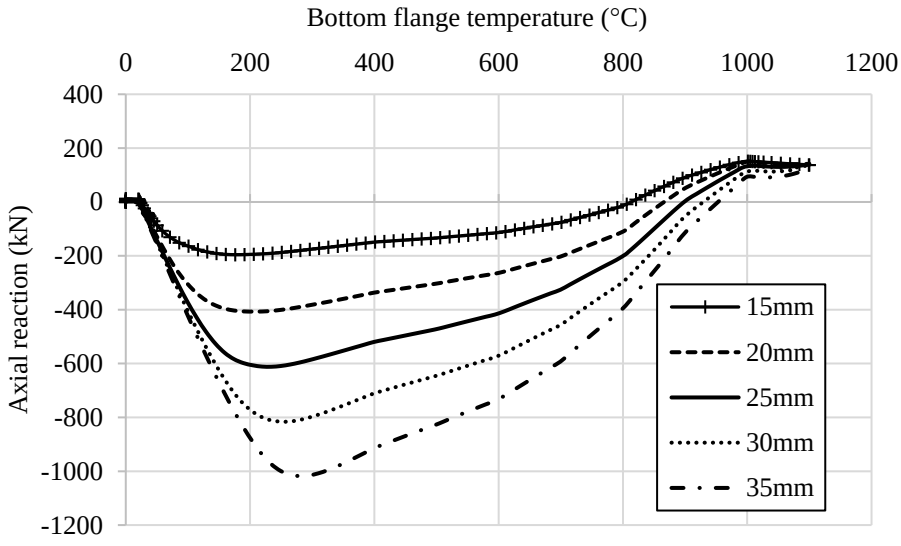

(b)

Figure 17 Influence of flange thickness on the elevated temperature behaviour of SSCWBs in terms of (a) the vertical deflection *versus* temperature and (b) the axial reaction *versus* temperature

5.4 Influence of web thickness

As stated before, the web in SSCWBs makes very little contribution towards either the flexural or axial stiffness of the section. Nevertheless, as it is a critical component of the cross-section, in this part of the parametric study, the relative influence of identical members with different web thicknesses is studied. Three different web thicknesses are examined, equal to 3, 5, 7, 9 and 12mm, all with a LR of 0.3 and axial restraint provided which is equal to 50% of the axial stiffness of the section. The results are presented in Fig. 18 and it is observed that the effect of web thickness on the vertical deflection and axial force behaviour of the examined SSCWBs is almost negligible. The axial force which develops in the section shows some very slight differences, with the SSCWB section with the thicker web (12 mm) able to resist slightly larger compressive forces, as expected.

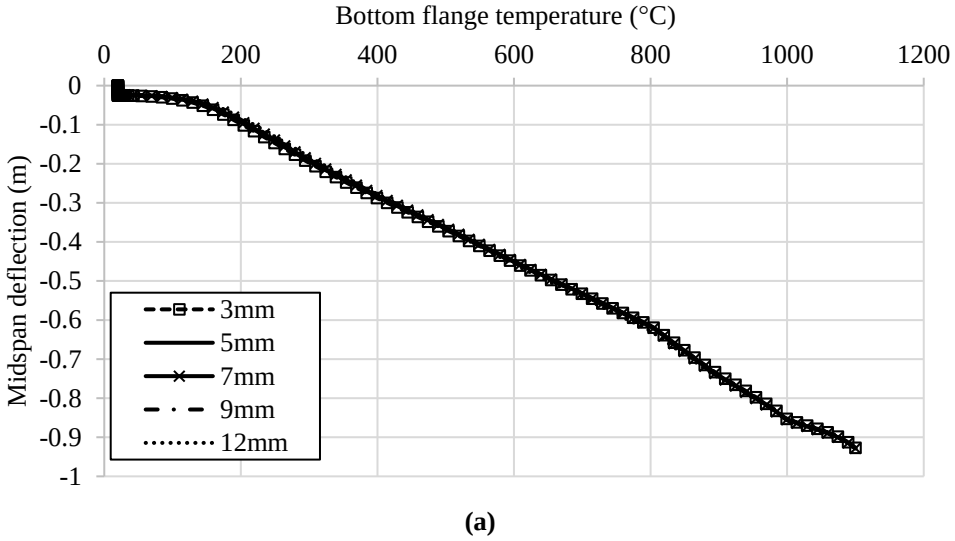

(a)

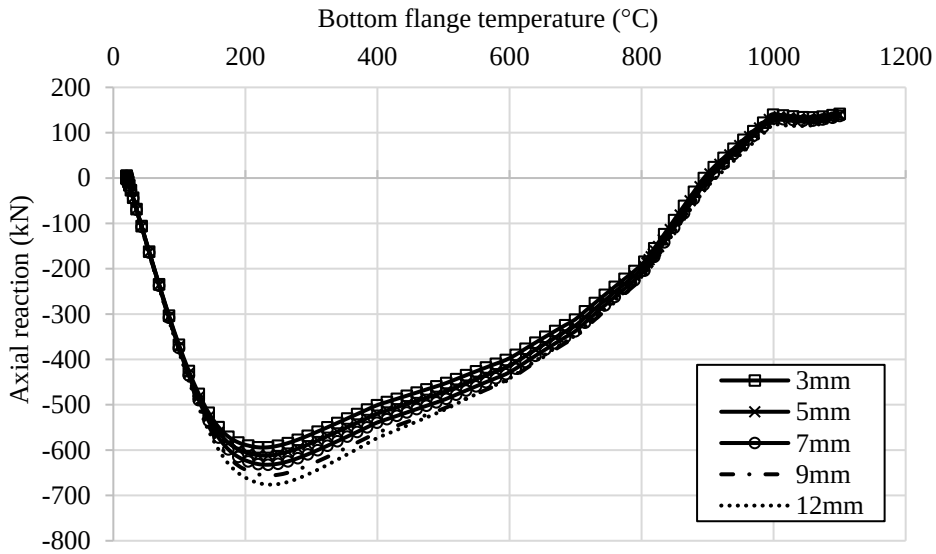

(b)

Figure 18 Influence of web thickness on the elevated temperature behaviour of SSCWBs in terms of (a) the vertical deflection *versus* temperature and (b) the axial force *versus* temperature

6. Analytical model for SSCWBs in fire

The results presented in earlier sections of this paper show that axially restrained SSCWBs under fire conditions have three main phases in their response. First, as the temperature increases, the beam tries to expand outwards in accordance with the coefficient of thermal expansion, and this is resisted by the axial restraint provided, thus inducing a compressive axial force in this section which continues until local buckling or yielding occurs. Then, secondly, as the temperature increases and the beam continues to deflect, and local buckling or yielding has developed in the beam, the compressive force in the section transitions to a tensile force and the overall load-carrying mechanism shifts from flexure to tensile catenary action. Finally, in the third phase, failure occurs under the ultimate tensile force. In order for engineers to be able to safely design SSCWBs for fire loading, it is useful and necessary to develop a tool that can reliably predict the temperature at which unloading of the compressive axial force begins, the transition temperature at which the load-carrying mechanism changes from flexure to tensile catenary action, as well as the temperature at which the ultimate tensile force is reached in the section. In this context, in the current section, an analytical model is developed to predict these key values, using the information gained from the FE modelling and parametric study previously described.

In this model, it is assumed that when the temperature of the restrained SSCWB is increased uniformly by $\Delta\theta$, an axial compressive force $N_{c,\theta}$ is induced in the beam. If k_A is the axial restraint stiffness, the free thermal strain ε_θ and the mechanical strain ε_m maybe determined using Eq. 3 and 4, respectively:

$$\varepsilon_\theta = \alpha(\Delta\theta) \tag{3}$$

$$\varepsilon_m = N_{c,\theta}/E_\theta A \tag{4}$$

where α is the coefficient of thermal expansion, A is the cross-sectional area of the SSCWB, $N_{c,\theta}$ is the axial compressive force and E_θ is the modulus of elasticity at temperature θ. It is important to note while calculating the cross-sectional area of the SSCWB, the web area is ignored as the contribution from the web towards the axial capacity is negligible.

The total strain in the beam ($\Delta L/L$, where ΔL is the total change in length and L is the original beam length) is determined as the sum of the mechanical and thermal strains which develop. The total strain $\Delta L/L$ is determined as:

$$\alpha(\Delta\theta) - N_{c,\theta}/E_\theta A = \Delta L/L = N_{c\theta}/k_A L \tag{5}$$

The temperature at which local buckling occurs in the beam and the runaway behaviour begins is calculated by applying the moment-axial force interaction relationship defined in Eq. 6, in accordance with the guidance given in Eurocode 3 Part 1-2 [5]:

$$N_{c,\theta}/N_{b,\theta} + k_y M/M_{c,\theta} \leq 1.0 \tag{6}$$

where M is the applied bending moment, $N_{b,\theta}$ is the flexural buckling resistance at elevated temperature, $M_{c,\theta}$ is the bending moment resistance at elevated temperature, and k_y is the interaction factor. In order to determine the transition temperature at which the beam starts to resist loads through tensile catenary action, the axial compressive force ($N_{c,\theta}$) is set to equal zero and, from Eq. 6, the applied bending moment (M) is set to equal the bending moment resistance of the section ($M_{c,\theta}$). In the final stage, as failure is approached, the applied bending moment (M) is carried entirely by tensile catenary action, in accordance with Eq. 7:

$$M = N_{T,max}\delta_v = k_{y,\theta} f_y A \delta_v \quad (7)$$

where δ_v is the maximum mid-span deflection of the beam. The maximum deflection under catenary action is calculated using Eq. 8, proposed by Najafi et al. [25], where l is half the total span of the beam (i.e. $L/2$) and ε_u is the maximum strain of the stainless steel:

$$\delta_v = l\sqrt{2\varepsilon_u} \quad (8)$$

It would be a conservative approach to choose the ultimate strain ε_u = 0.2 as this would result in lower values of $k_{y,\theta}$ and very high values of the corresponding temperature [25]. From the FE analysis, a value of ε_u = 0.1 is found to be appropriate for accurate predictions of the maximum vertical deflection in the beam. From Eq. 9, the yield strength reduction factor ($k_{y,\theta}$) is determined, and the corresponding temperature θ is determined based on this reduction factor.

$$k_{y,\theta} = \frac{M}{f_y A \delta_v} \quad (9)$$

The results obtained from the FE parametric study previously described are compared with the predictions from the analytical model (AM) and the results are presented in Table 1, including the temperature at which runaway behaviour begins ($\theta_{Nc,max}$), the transition temperature (θ_T) and the temperature at which the ultimate tensile failure load is reached ($\theta_{Nt,max}$). Three different load levels are included in the table, including LRs equal to 0.3, 0.5 and 0.7. It is shown that the proposed model is capable of predicting all of these key temperatures accurately.

Table 1 Comparison of the key temperatures at various stages of the response from the FE model and the analytical model

	$\theta_{Nc,max}$			θ_T			$\theta_{Nt,max}$		
Axial Restraint	FE	AM	|FE-AM|	FE	AM	|FE-AM|	FE	AM	|FE-AM|
LR = 0.3									
5%	670	659	11	916	902	14	1089	1099	10
10%	505	500	5	909	902	7	1094	1099	5
30%	279	248	31	903	902	1	1090	1099	9
50%	224	198	26	901	902	1	1096	1099	3
70%	189	169	20	899	902	3	1090	1099	9
100%	149	139	10	895	902	7	1098	1099	1
LR = 0.5									

5%	550	562	12	826	816	10	1000	1000	0
10%	369	381	12	821	816	5	1004	1000	4
30%	231	195	36	817	816	1	1004	1000	4
50%	165	150	15	811	816	5	999	1000	1
70%	150	125	25	810	816	6	1000	1000	0
100%	125	116	9	810	816	6	999	1000	1
LR = 0.7									
5%	380	400	20	699	735	36	989	945	44
10%	264	275	11	700	735	35	989	945	44
30%	165	150	15	697	735	38	987	945	42
50%	140	111	29	695	735	40	988	945	43
70%	120	96	24	699	735	36	986	945	41
100%	106	88	18	697	735	38	987	945	42

7. Conclusions

This paper presents a detailed investigation into the behaviour of stainless-steel corrugated web beams (SSCWBs) under elevated temperature. The increase in popularity of stainless steel as a structural material is well known and is largely owing to its durability and excellent sustainability credentials. In addition, and critically in the context of this paper, structural stainless steel generally behaves better than carbon steel in fire conditions. Simultaneously, corrugated web beams have also become increasingly popular for long-spanning structural elements in a range of applications, as the buckling strength of the web is improved through the corrugated web plates. To date, there has been no study into corrugated web beams made from stainless steel in fire conditions.

In this paper, a FE model is developed which can accurately and reliably depict the behaviour of SSCWBs under fire conditions. In the absence of experimental data for these types of members, the model is validated using the two different sets of data including (i) the test results presented by Liu et al. [32] on restrained carbon steel beams and (ii), the numerical data presented by Wang et al. [20] on the fire response of carbon steel corrugated web beams (CSCWBs). Together, these data sets capture all of the key behavioural aspects of the response of SSCWBs, and the results are used to verify different aspects of the modelling approach, such as the element type, mesh size, boundary conditions, and solution process. The validated model is then employed to conduct a large number of simulations, looking at the influence of several key parameters on the response, and also to understand the key characteristics of the overall performance. Finally, an analytical model to predict the temperatures at which these key characteristic events occur is proposed.

The following conclusions are observed based on the results presented:

- The catenary action in SSCWBs is delayed compared to CSCWBs due to their improved performance in terms of strength and stiffness retention at elevated temperature. Therefore, SSCWBs are capable of withstanding comparatively higher temperatures compared to CSCWBs.

- Both SSFWBs (with a flat web) and SSCWBs (with a corrugated web) show similar flexural performance to each other. On the other hand, the axial behaviour is significantly different in terms of the maximum axial compression which develops in the sections. The SSFWBs are able to resist greater axial compressive loads compared with similar SSCWBs owing to the greater axial stiffness of these cross-sections.

- In the early stages of a fire, the midspan deflection behaviour of SSCWBs is greatly influenced by the level of axial restraint which is provided to the beam, while as the member approaches the transition temperature, the behaviour is mainly governed by the retention of mechanical properties such as strength and stiffness, of the stainless steel.

- When SSCWBs are subjected to relatively high load ratios, tensile catenary action develops sooner compared with more lightly-loaded beams.

- The axial force *versus* temperature behaviour of SSCWBs is greatly affected by the flange thickness, while the web thickness is of negligible influence.

- The analytical model presented is shown to accurately predict various stages of the behaviour of SSCWBs, i.e., the onset of local buckling, the transition temperature, and the temperature at which ultimate tensile failure occurs.

Declaration of Conflicting Interests

The author(s) declared no potential conflicts of interest with respect to the research, authorship, and/or publication of this article.

Acknowledgements

The work reported in this paper has formed part of the SureFire project (T22-505/19-N) funded by the Research Grants Council Hong Kong under its Theme-based Research Scheme. This research is also funded by the RGC Hong Kong GRF Scheme and HK PolyU. The authors also acknowledge the additional support provided by the Hong Kong Polytechnic University for this Project.

References

[1] ISSF, Built to Last - Stainless Steel as an Architectural Material, Int. Stainl. Steel Forum. (2015).
[2] N.R. Baddoo, Stainless steel in construction: A review of research, applications, challenges and opportunities, J. Constr. Steel Res. 64 (2008) 1199–1206. https://doi.org/10.1016/j.jcsr.2008.07.011.
[3] L. Gardner, The use of stainless steel in structures, Prog. Struct. Eng. Mater. 7 (2005) 45–55. https://doi.org/10.1002/pse.190.
[4] L. Gardner, R.B. Cruise, C.P. Sok, K. Krishnan, J. Ministro Dos Santos, Life-cycle

costing of metallic structures, Proc. Inst. Civ. Eng. - Eng. Sustain. 160 (2007) 167–177. https://doi.org/10.1680/ensu.2007.160.4.167.
[5] EN 1993-1-2, Eurocode 3: Design of steel structures - Part 1-2: General rules - Structural fire design, Eur. Commitee Stand. (2005).
[6] Z. Xing, O. Zhao, M. Kucukler, L. Gardner, Fire testing and design of slender stainless steel I-sections in weak-axis flexure, Thin-Walled Struct. 171 (2022) 108682. https://doi.org/10.1016/j.tws.2021.108682.
[7] Z. Xing, M. Kucukler, L. Gardner, Local buckling of stainless steel I-sections in fire: Finite element modelling and design, Thin-Walled Struct. 161 (2021) 107486. https://doi.org/10.1016/j.tws.2021.107486.
[8] Zeman & Co GesellschaftmbH, Corrugated web beam, Tech. Doc. (2003) 1–74.
[9] M. Elgaaly, A. Seshadri, R.W. Hamilton, Bending Strength of Steel Beams with Corrugated Webs, J. Struct. Eng. 123 (1997) 772–782. https://doi.org/10.1061/(asce)0733-9445(1997)123:6(772).
[10] M. Elgaaly, R.W. Hamilton, A. Seshadri, Shear Strength of Beams with Corrugated Webs, J. Struct. Eng. 122 (1996) 390–398. https://doi.org/10.1061/(asce)0733-9445(1996)122:4(390).
[11] R.G. Driver, H.H. Abbas, R. Sause, Shear Behavior of Corrugated Web Bridge Girders, J. Struct. Eng. 132 (2006) 195–203. https://doi.org/10.1061/(asce)0733-9445(2006)132:2(195).
[12] R. Luo, B. Edlund, Shear capacity of plate girders with trapezoidally corrugated webs, Thin-Walled Struct. 26 (1996) 19–44. https://doi.org/10.1016/0263-8231(96)00006-7.
[13] R. Luo, B. Edlund, Buckling analysis of trapezoidally corrugated panels using spline finite strip method, Thin-Walled Struct. 18 (1994) 209–224. https://doi.org/10.1016/0263-8231(94)90019-1.
[14] L. Laím, H.D. Craveiro, R. Simões, A. Escudeiro, A. Mota, Experimental analysis of cold-formed steel columns with intermediate and edge stiffeners in fire, Thin-Walled Struct. 146 (2020). https://doi.org/10.1016/j.tws.2019.106481.
[15] M.A. Shaheen, S. Afshan, A.S.J. Foster, Performance of axially restrained carbon and stainless steel perforated beams at elevated temperatures, Adv. Struct. Eng. 24 (2021) 3564–3579. https://doi.org/10.1177/13694332211033965.
[16] J. Yang, Y. Shi, W. Wang, L. Xu, H. Al-azzani, Experimental and numerical studies on axially restrained cold-formed steel built-up box columns at elevated temperatures, J. Constr. Steel Res. 171 (2020) 106143. https://doi.org/10.1016/j.jcsr.2020.106143.
[17] H. Al-azzani, J. Yang, A. Sharhan, W. Wang, A Practical Approach for Fire Resistance Design of Restrained High-Strength Q690 Steel Beam Considering Creep Effect, Fire Technol. 57 (2021) 1683–1706. https://doi.org/10.1007/s10694-020-01078-7.
[18] H.-Y. Kim, B.-Y. Cho, H.-J. Kim, H. Kang, K.-S. Kim, Experimental Study on the Fire Resistance Performance of Prestressed Composite Beam with Corrugated Web, J. Korean Soc. Hazard Mitig. 14 (2014) 35–41. https://doi.org/10.9798/kosham.2014.14.1.35.
[19] M.M. Maslak, M. Lukacz, Interactive shear resistance of corrugated web in steel beam exposed to fre, J. Struct. Fire Eng. 7 (2016) 69–78. https://doi.org/10.1108/JSFE-03-2016-006.
[20] P. Wang, C. Liu, M. Liu, Large deflection behavior of restrained corrugated web steel beams in a fire, J. Constr. Steel Res. 126 (2016) 92–106. https://doi.org/10.1016/j.jcsr.2016.07.017.

[21] P. Wang, C. Liu, M. Liu, X. Wang, Numerical studies on large deflection behaviour of axially restrained corrugated web steel beams at elevated temperatures, Thin-Walled Struct. 98 (2016) 58–74. https://doi.org/10.1016/j.tws.2015.04.028.
[22] Y.Z. Yin, Y.C. Wang, Analysis of catenary action in steel beams using a simplified hand calculation method, Part 2: Validation for non-uniform temperature distribution, J. Constr. Steel Res. 61 (2005) 213–234. https://doi.org/10.1016/j.jcsr.2004.07.003.
[23] Y.Z. Yin, Y.C. Wang, Analysis of catenary action in steel beams using a simplified hand calculation method, Part 1: Theory and validation for uniform temperature distribution, J. Constr. Steel Res. 61 (2005) 183–211. https://doi.org/10.1016/j.jcsr.2004.07.002.
[24] M. Najafi, Y.C. Wang, Axially restrained steel beams with web openings at elevated temperatures, Part 1: Behaviour and numerical simulation results, J. Constr. Steel Res. 128 (2017) 745–761. https://doi.org/10.1016/j.jcsr.2016.10.002.
[25] M. Najafi, Y.C. Wang, Axially restrained steel beams with web openings at elevated temperatures, Part 2: Development of an analytical method, J. Constr. Steel Res. 128 (2017) 687–705. https://doi.org/10.1016/j.jcsr.2016.10.003.
[26] M. Ali Khan, K.A. Cashell, A.S. Usmani, Analysis of Restrained Composite Perforated Beams during Fire Using a Hybrid Simulation Approach, J. Struct. Eng. (United States). 146 (2020) 1–15. https://doi.org/10.1061/(ASCE)ST.1943-541X.0002528.
[27] M.A. Khan, L. Jiang, K.A. Cashell, A. Usmani, Virtual hybrid simulation of beams with web openings in fire, J. Struct. Fire Eng. (2019). https://doi.org/10.1108/JSFE-01-2019-0008.
[28] M.A. Khan, L. Jiang, K.A. Cashell, A. Usmani, Analysis of restrained composite beams exposed to fire using a hybrid simulation approach, Eng. Struct. 172 (2018) 956–966. https://doi.org/10.1016/j.engstruct.2018.06.048.
[29] ABAQUS, ABAQUS Documentation, Dassault Systèmes, U.S.A., (2010).
[30] N. Lopes, P. Vila Real, L. Simões Da Silva, J.M. Franssen, Numerical analysis of stainless steel beam-columns in case of fire, Fire Saf. J. 50 (2012) 35–50. https://doi.org/10.1016/j.firesaf.2012.02.003.
[31] Y. Huang, B. Young, Structural performance of cold-formed lean duplex stainless steel beams at elevated temperatures, Thin-Walled Struct. 129 (2018) 20–27. https://doi.org/10.1016/j.tws.2018.03.031.
[32] T.C.H. Liu, M.K. Fahad, J.M. Davies, Experimental investigation of behaviour of axially restrained steel beams in fire, J. Constr. Steel Res. 58 (2002) 1211–1230. https://doi.org/10.1016/S0143-974X(01)00062-1.
[33] A. Pournaghshband, S. Afshan, M. Theofanous, Elevated temperature performance of restrained stainless steel beams, Structures. 22 (2019) 278–290. https://doi.org/10.1016/j.istruc.2019.08.015.
[34] CECS291:2011, Technical Specification for Steel Structures with Corrugated Webs, in: China Plan. Press, Beijing, 2011.
[35] K.A. Cashell, M. Malaska, M. Khan, M. Alanen, K. Mela, Numerical analysis of the behaviour of stainless steel cellular beam in fire, Ce/Papers. 3 (2019) 895–900. https://doi.org/10.1002/cepa.1150.
[36] K.A. Cashell, M. Malaska, M. Khan, M. Alanen, K. Mela, Experimental and numerical analysis of stainless steel cellular beams in fire, Fire Saf. J. 121 (2021). https://doi.org/10.1016/j.firesaf.2021.103277.
[37] EN 1991-1-2, Eurocode 1: Actions on structures - Part 1-2: General actions - Actions

on structures exposed to fire, Eur. Commitee Stand. (2005).
[38] H. Yang, F. Liu, L. Gardner, Performance of concrete-filled RHS columns exposed to fire on 3 sides, Eng. Struct. 56 (2013) 1986–2004. https://doi.org/10.1016/j.engstruct.2013.08.019.
[39] SCI, Design manual for structural stainless steel, Silwood Park. Ascot, Berksh. (2017).